Rueda-García, L.; Bonet Senach, JL.; Miguel Sosa, P.; Fernández Prada, MÁ. (2022). Experimental study on the shear strength of reinforced concrete composite T-shaped beams with web reinforcement. Engineering Structures. 255:1-17. https://doi.org/10.1016/j.engstruct.2022.113921

Experimental study on the shear strength of reinforced concrete composite T-shaped beams with web reinforcement

Lisbel Rueda García, lisruega@cam.upv.es

José Luis Bonet Senach, jlbonet@cst.upv.es

Pedro Fco. Miguel Sosa, pmiguel@cst.upv.es

Miguel Ángel Fernández Prada, mafernan@cst.upv.es

Universitat Politècnica de València, Camí de Vera s/n, 46022, Valencia, Spain

Abstract

The current increasing use of precast concrete elements and cast-in-place concrete slabs, namely concrete composite elements, in construction requires a better understanding of their behaviour in shear. In this work, 19 T-shaped composite and monolithic specimens failing in shear were experimentally tested. Their results were compared to study the influence on the shear strength of: the flange width, the presence of an interface between concretes and the strength of the concretes of both beam and slab. The shear transfer mechanisms were analysed by adapting to these specimens a mechanical model previously proposed by the authors for rectangular composite beams. It was concluded that: the composite specimens' shear strength did not increase with widening flange width when the specimens showed an extended interface cracking, but increased when their crack pattern was similar to that of the monolithic specimens; the presence of an interface decreased the shear strength; the slab's concrete compressive strength modified the composite specimens' shear strength when the slab failed in shear, but not when the slab failed in bending or when the interface failed. The shear formulations of EC2, MC-10 Level III and ACI 318-19 gave good estimations when using the weighted average of the compressive strengths of the beam and slab concretes, similarly to those obtained with the proposed

model. From the experimental results, the improvement of the interface shear strength of composite beams is proposed as a practical recommendation for increasing their shear strength. At the same time, the slab width and the slab's concrete strength could be increased with the same purpose. This work experimental findings and the adaptation of the mechanical model to T-shaped beams lay the groundwork for a future development of a shear design and assessment formulation for concrete composite elements.

Keywords: precast construction, reinforced concrete, composite beam, T-shaped beam, shear strength, shear failure, mechanical behaviour, design, assessment.

Highlights

- Monolithic and composite T-shaped beams with stirrups were tested in shear
- The flange-web horizontal interface modified the shear strength mechanism
- Flanges did not increase shear strength in beams with an extended interface cracking
- Composite beams' shear strength decreased compared to monolithic beams
- The proposed model well matches this test programme's experimental results

1. Introduction

Currently a clear trend towards prefabricated construction with reinforced concrete elements is seen. The use of precast concrete beams in building structures, bridges, etc., only requires employing a layer of cast-in-place concrete to ensure structural integrity [1], which results in structural elements known as concrete composite beams. This type of composite construction is present in many structures like building floors or bridge decks [2,3]. Given the vast number of these composite structures, it is important to study their structural behaviour to reduce design and maintenance costs. Currently, the contribution of cast-in-place slab to shear strength in composite beams is often neglected in the design and assessment of existing structures, but its consideration can imply substantial cost savings for these infrastructures [4,5].

While interface shear strength has been widely studied in composite beams [6–11], their vertical shear strength has not been analysed in depth [4]. Experimental analyses of full-scale composite specimens with web reinforcement can be found in the literature [12–20], but they do not analyse either the contribution of slab to shear strength or the influence of the interface between concretes on shear strength. Current codes (like EC2 [21] and MC-10 [22]) do not clarify how to account for the slab in the shear strength of composite elements. Only ACI 318-19 [23] specifies how composite specimens' shear strength can be calculated: using the properties of the element (precast beam or cast-in-place slab) that result in the most critical shear strength value or the properties of individual elements. Nevertheless, relevant experimental and theoretical evidence are still needed to support the validity of these considerations for composite specimens [1,4].

A previous study by the authors [24] analysed the contribution of cast-in-place slab to shear strength in concrete composite beams with rectangular cross-sections and web reinforcement. For the specimens of this experimental programme, it was concluded that slab increased shear strength. Thus, neglecting its contribution to shear strength was too

conservative. Besides, the interface between concretes significantly modified shear behaviour in comparison to monolithic specimens. This study of the shear strength mechanisms derived in the proposal of a mechanical model that analyses test specimens' behaviour.

In precast concrete structures, composite beams with T-shaped cross-sections are often employed, such as bridge decks consisting of precast concrete beams and cast-in-place slabs, beam-and-block floors, rib-and-slab floors with precast reinforced concrete beams or connections of precast floor slabs (e.g., hollow-core slabs) supported by precast beams, where the free space is filled with *in situ* concrete [2,3]. Some examples appear in Fig. 1.

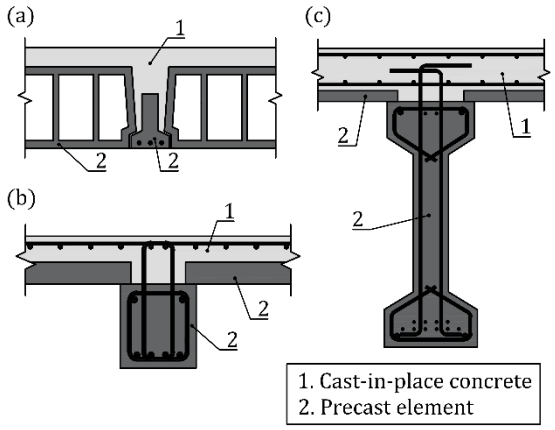

Fig. 1. Examples of reinforced concrete composite T-shaped elements in precast construction: (a) beam-and-block floor; (b) connection of precast beam and hollow-core slab filled with cast-in-place concrete; (c) precast bridge girder with cast-in-place slab.

Although the increased shear strength provided by flanges in monolithic T-shaped concrete beams has been traditionally and widely studied [25–32], and the literature offers several models for the distribution of tangential stresses in flanges [27,30,32–38], no experimental studies that analyse the influence of flanges on the shear strength of T-shaped concrete composite beams appear in the literature despite the many structural elements built with this typology in practice [2].

The aim of the present experimental programme is to study the shear strength of T-shaped reinforced concrete composite beams with shear reinforcement, consisting of a rectangular precast beam and a cast-in-place slab on top. For this purpose, 19 T-shaped reinforced

concrete specimens were tested in shear with the following variable parameters: flange width, presence of an interface between concretes, and beam and slab's concrete strengths. An in-depth study of the shear strength mechanisms and failure modes of the specimens of this experimental programme was conducted by adapting to the specimens of this programme the lower-bound plasticity-based model proposed in [24], which explained the results obtained on the influence of the studied parameters. Parameters were analysed by comparing specimens to one another, and also to the rectangular specimens of the previous study carried out by the authors in [24]. Current codes formulations for shear strength were also verified with the experimental results.

The present research work contributes to: increase the number of available experimental tests on concrete composite beams; study the contribution of the cast-in-place slab to concrete composite beams' shear strength by analysing different variables and mechanical behaviour; extend the mechanical model proposed by the authors to T-shaped composite elements; verify current codes' shear design provisions.

2. Materials and methods

2.1. Test parameters

The three variable parameters selected to analyse the shear behaviour of the T-shaped composite beams with web reinforcement are the following:

- Flange width. Two flange widths were studied in this work. First, the one of type C cross-section, that equalled flange depth, since multiple publications observed that the maximum contribution of flanges to shear strength is given by that width [25,32,33]. Second, the one of type D cross-section, whose flange width was twice the flange depth (Fig. 2), to verify in the specimens of this experimental programme that limit in the contribution of flanges observed by previous authors. Furthermore, the test results from these specimens can be compared to those provided by the

authors in a previous work [24] for rectangular sections (type B series) as these specimens have the same web width and height as those of the type C and D series.

- Presence of an interface between concretes. The specimens of series C1 and D1 were monolithic (without interface), while the concretes of the beam and slab were cast at different times in the specimens of series C2 and D2 (with the interface) (Fig. 2).
- Beam and slab concretes' compressive strengths. Two different concrete strengths were used for the precast beams: normal-strength concrete (NSC), with a design compressive strength of 30 MPa, and concrete with higher compressive strength (HCS), with a design compressive strength of 50 MPa. For slabs, only an NSC with a design compressive strength of 30 MPa was used.

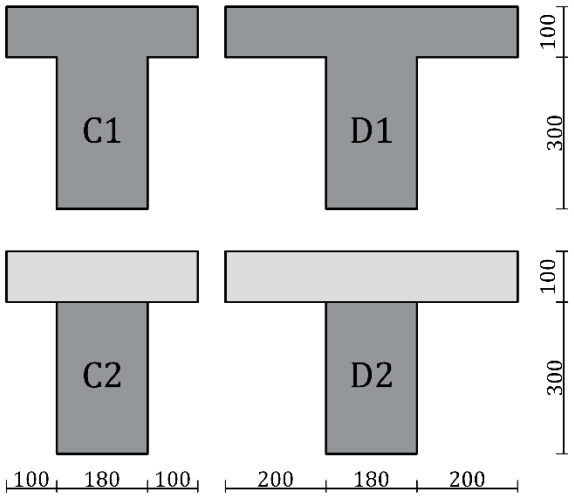

Fig. 2. Cross-section types (dimensions: mm).

2.2. Test specimens

This experimental programme consists of 19 T-shaped beams with web reinforcement. Table 1 shows the number of specimens of each cross-section type and the types of concrete used for the precast beam and the cast-in-place slab. The nomenclature of each specimen, *xWPyzk(j),* was analogous to that of a previous study performed by the authors for rectangular beams [24] to allow a comparison of specimens, where:

- "*xW*" refers to the name of the series: NW stands for the specimens with NSC in the precast beam and HW stands for the specimens with HCS in the precast beam.
- "*Py*" refers to the concrete pouring batch: from P2 to P7, as the fabrication process of these specimens was conducted 6 times. They were the same batches as in [24].
- "*z*" refers to the cross-section type (C or D in Fig. 2).
- "*k*" refers to the number of concretes that formed the specimen: 1 for monolithic beams, 2 for composite beams.
- "*j*" ("a" or "b") is used only when more than one specimen with the same previously described characteristics was fabricated.

Table 1. Series of the experimental programme.

Series	Type of beam's concrete	Type of slab's concrete	Number of specimens per cross-sectional type			
			C1	C2	D1	D2
NW	NSC	NSC	3	3	2	3
HW	HCS	NSC	2	2	2	2

The dimensions of specimens and their reinforcement are shown in Fig. 3. They were designed to emulate real precast beams with cast-in-place slabs used in practice, like those shown in Fig. 1b-c, but simplified to focus the test programme on the study of the test parameters defined in Section 2.1. All the specimens were 3.50 m long. The distance between supports was 2.74 m. Two-point loads with a 0.40 m distance between them were applied, which formed two spans: a 1.34-metre long principal span in which failure was expected; a 1.00-metre long span, which was reinforced to avoid its shear failure.

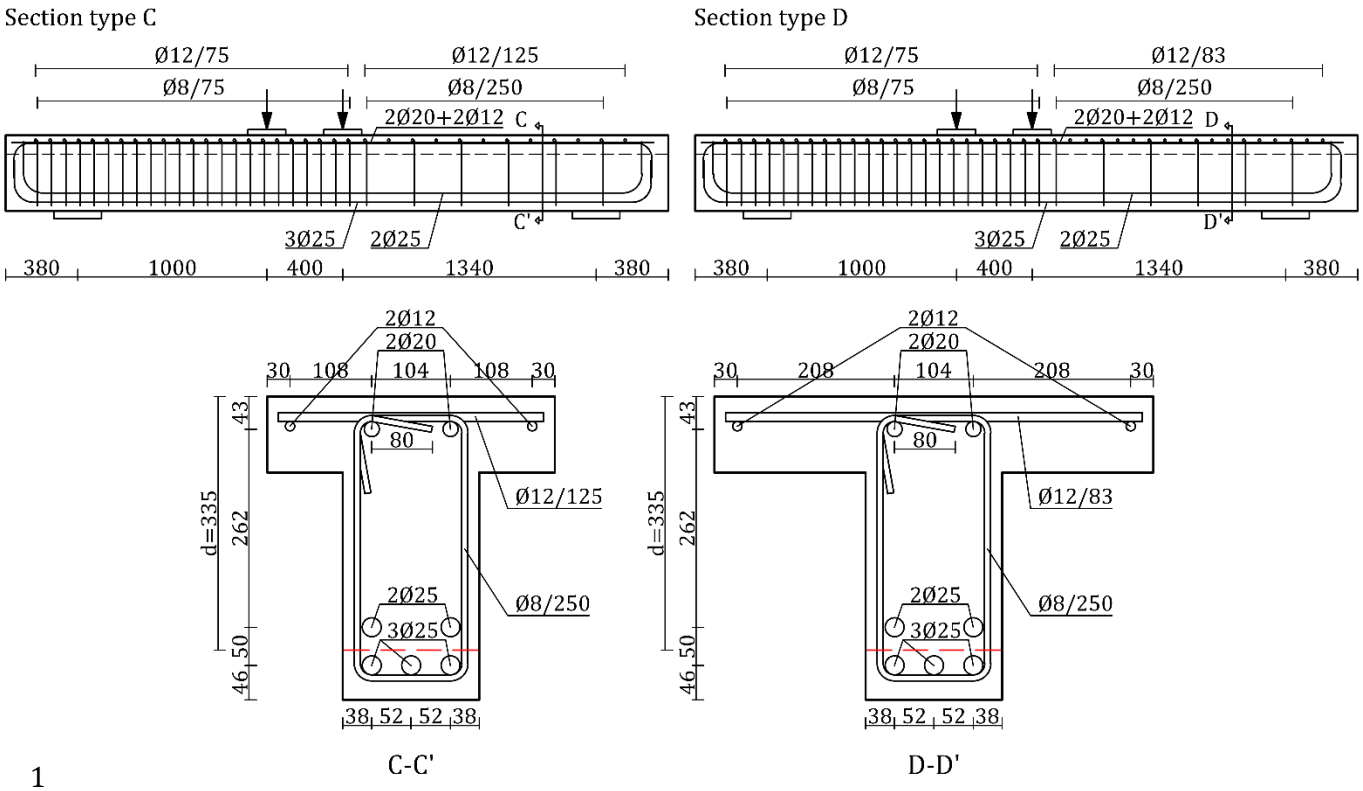

Fig. 3. Dimensions and reinforcement of beams type C and D (dimensions in mm).

In the composite specimens (C2 and D2), the precast beam was 0.30 m high (see Fig. 2) and the cast-in-place slab was 0.10 m high.

All the specimens had fixed the following characteristics to make them comparable between them: a 4.0% longitudinal reinforcement ratio (ρ_l) to avoid bending failure in all the specimens, including those with the widest flange; a shear reinforcement ratio (ρ_w) of 0.22%, which met the maximum spacing requirements between stirrups of all the design codes considered in this study [21–23]; a shear span-effective depth ratio (a/d) of 4.0, which was selected to foster shear failure governed mainly by beam shear-transfer actions [28,39]. The beam's concrete surface underwent no further treatment after vibration. The interface roughness and the shear reinforcement ratio were selected as a result of a previous study carried out by the authors [40], which showed that they were suitable for diagonal beam cracking to develop before interface cracking. Finally for the composite specimens, the time elapsed between pouring the beam concrete and the slab concrete was 1 day. This time was set because a previous study by the authors [24] proved that, for the

specimens of this experimental programme, marked differential shrinkage between the beam and slab concretes did not significantly change specimens' vertical shear strength.

2.3. Fabrication of specimens

Specimens were fabricated in six batches (fabrication batches P2 to P7 in Table 2) to compare the specimens from the same batch with identical concrete strength. The fabrication process of each batch was conducted on 2 consecutive days. On the first day, the concrete of the monolithic specimens and the precast beams of the composite specimens was poured. In the composite specimens, the interface between the concretes in the principal span, where failure was expected, was not further treated after vibration. Thus interface roughness was "as cast" or "smooth" according to current codes [21–23] (see Fig. 4). In the reinforced span, the interface was raked before concrete hardened to obtain a "very rough" interface as defined in the codes. The interface shear strength of the reinforced span was increased in this way. The measured slump of the beam's concrete, which can influence surface roughness [24], is shown in Table 2. The slump test was conducted in accordance with UNE-EN 12350-2 [41].

Table 2. Summary of the test results.

Series	Fabrication batch	Specimen	$f_{c,28,b}$ (MPa)	$f_{c,28,s}$ (MPa)	$f_{c,b}$ (MPa)	$f_{c,s}$ (MPa)	$E_{c,b}$ (MPa)	$E_{c,s}$ (MPa)	$f_{ct,b}$ (MPa)	$f_{ct,s}$ (MPa)	Slump beam (cm)	V_{exp} (kN)
NW	P2	NWP2C1	37	-	39	-	31961	-	2.83	-	17.5	221
		NWP2C2		34	38	34	33977	30756	3.02	2.88		177
		NWP2D2		34	38	34	33977	30756	3.02	2.88		216
	P3	NWP3C1	32	-	33	-	32927	-	2.58	-	22.5	187
		NWP3C2		38	32	37	32927	33854	2.58	3.21		172
		NWP3D2		38	31	38	32927	33854	2.58	3.21		176
	P4	NWP4C1	39	-	39	-	28300	-	2.86	-	18.0	200
		NWP4C2		33	39	33	28652	27606	2.79	2.80		197
		NWP4D2		33	40	33	28476	28715	3.04	2.48		229
	P7	NWP7D1a	24	-	24	-	22925	-	1.90	-	15.0	195
		NWP7D1b		-	24	-	22925	-	1.90	-		197
HW	P5	HWP5C1	43	-	42	-	24662	-	2.40	-	20.0	238
		HWP5C2		22	44	21	26936	20344	2.58	2.01		166
		HWP5D1		-	42	-	24662	-	2.40	-		200
		HWP5D2		22	44	21	26936	20344	2.58	2.01		173
	P6	HWP6C1	52	-	52	-	28395	-	2.86	-	24.0	231
		HWP6C2		36	52	36	28395	29458	2.86	3.01		222
		HWP6D1		-	52	-	28651	-	2.86	-		246
		HWP6D2		36	52	36	28395	29458	2.86	3.01		209

Notation: suffix "b" refers to the beam's concrete; suffix "s" refers to the slab's concrete.
Average coefficients of variation of measurements: 2% for $f_{c,28}$ and f_c; 3% for E_c; 7% for f_{ct}.

Fig. 4. "As cast" interface appearance before the cast-in-place slab's concrete casting.

On the second day, the concrete of the composite specimens' slab was poured. The entire length of beams was laid on the floor during this concrete casting. Hence, in this experimental programme, the beam and slab of the composite specimens were loaded at the same time.

2.4. Material properties

Table 2 shows the 28-day compressive strength of concretes ($f_{c,28}$), and the compressive strength (f_c), modulus of elasticity (E_c) and tensile strength (f_{ct}) of the concretes at the testing age, which were obtained by averaging the test results over two cylindrical specimens (300 mm high, 150 mm diameter) according to UNE-EN 12390 [42–44]. Tensile concrete strength was obtained as 90% of concrete's tensile splitting strength, as described in [45]. The average coefficient of variation values of measurements are also indicated in Table 2.

Regarding concrete mixture composition, the NSC concretes had a water-cement ratio of 0.52, the amount of Portland cement was 325 kg/m^3 and a maximum aggregate size of 10 mm. The same parameters for HCS were 0.44, 500 kg/m^3 and 10 mm, respectively.

Table 3 shows the mechanical properties of reinforcing steel, which were obtained as indicated in UNE-EN ISO 6892 [46]. The results were the average of two tests for each nominal diameter. The steel used for all the bars was type C according to EC2 [21].

Table 3. Average values of the transverse and longitudinal reinforcement properties.

	Series	$\emptyset$ (mm)	f_y (MPa)	E_s (GPa)	ε_y (‰)	f_u (MPa)	ε_u (%)
Stirrups	All series	8	538	203	2.7	658	12.0
Longitudinal and slab's transverse reinforcement	NWP2, NWP3, NWP4	12	533	207	2.6	638	13.3
		20	585	192	3.1	673	41.0
		25	557	199	2.8	666	48.3
	NWP7, HWP5	12	529	196	2.7	651	30.3
		20	541	194	2.8	654	26.7
		25	548	235	2.3	658	21.6
	HWP6	12	527	201	2.6	657	29.9
		20	560	190	2.9	675	22.0
		25	574	237	2.4	687	19.2

2.5. Instrumentation

The instrumentation arranged in specimens consisted of: load cells, strain gauges and linear variable displacement transformers (LVDTs). Three 1000 kN load cells were used to measure the forces at the two bearing points and the hydraulic jack. Strain gauges of 2 mm

measuring length and 120 Ω resistance were placed on some reinforcing bars: G1 to G6 (see Fig. 5a) on the tension longitudinal reinforcement at three different cross-sections (Sections A, B and C); G7 and G8 on the compression longitudinal reinforcement at Section C; G9 to G16 at the mid-length of the two legs of stirrups w3 to w6 (Fig. 5a). Three strain gauges of 60 mm measuring length and 120 Ω resistance were located on the top concrete surface at Sections A and B (gauges C1 to C6 in Fig. 5a). Their locations at type C and D cross-sections are shown in Fig. 5b. Finally, five LVDTs (V1 to V5 in Fig. 5c) were placed on the concrete surface to measure vertical displacements, two LVDTs (O1 and O2) were fixed to the top and bottom of beams to detect the beginning of cracking, and four LVDTs (H1 to H4) were fixed to the web and flange to measure the horizontal slip between them. In all the tests, two digital cameras took pictures at a rate of 0.5 Hz and a synchronised recording system was used so that each photogram was assigned to the corresponding applied load. A high-speed camera was employed to record brittle failures and to detect the beginning of cracking.

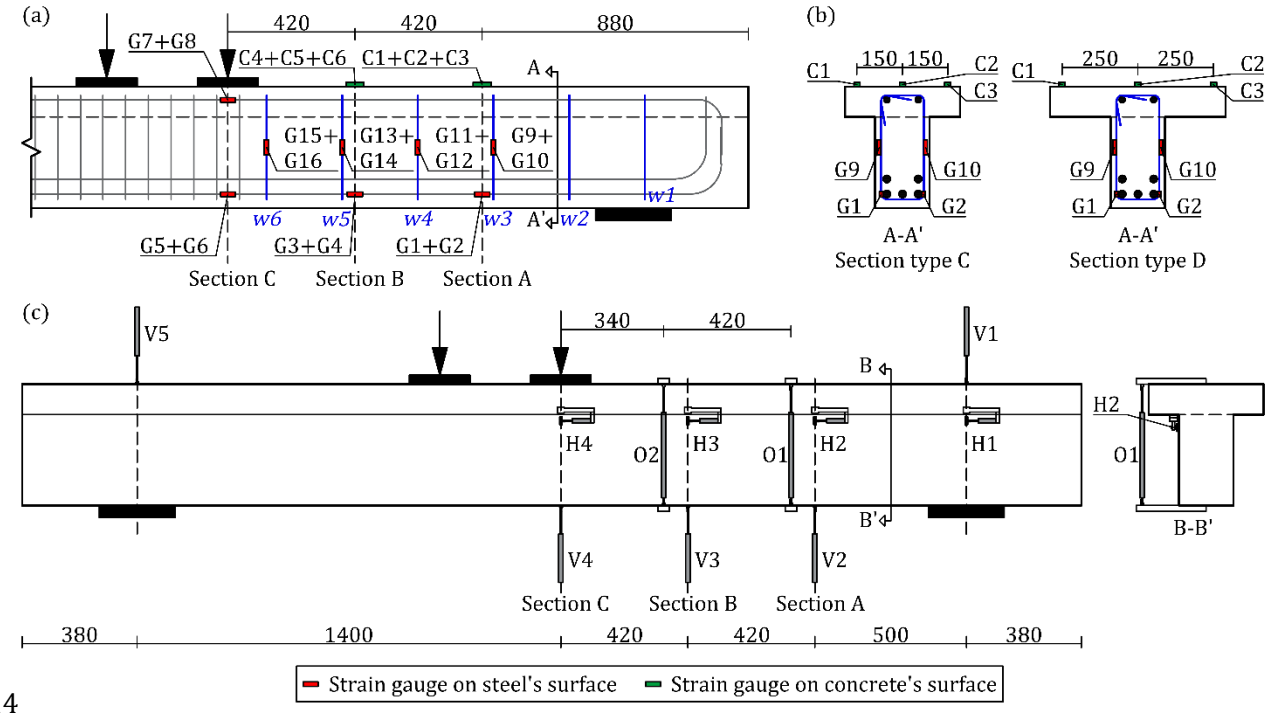

Fig. 5. Instrumentation of the test specimens: (a) strain gauges at the principal span; (b) strain gauges at section A-A' for beams type C and D; (c) LVDTs (dimensions in mm).

2.6. Test setup and procedure

Tests were performed in the same way as in the authors' previous studies [24,47], in which the steel loading frame shown in Fig. 6 was used. A 1200 kN hydraulic jack applied the vertical load with displacement control at a speed of 0.02 mm/s. Load was divided into two point loads by means of the steel frame shown in Fig. 6, which had a hinge to maintain load in a vertical direction, even if the upper beam plane was not horizontal due to its deformation. Two steel plates (200x200x30 mm) centred on the slab width transmitted the load from the steel frame to specimens. The beam's two bearing points consisted of a steel plate 250 mm width, a ball bed to eliminate the horizontal reaction and a hinge to allow for rotations.

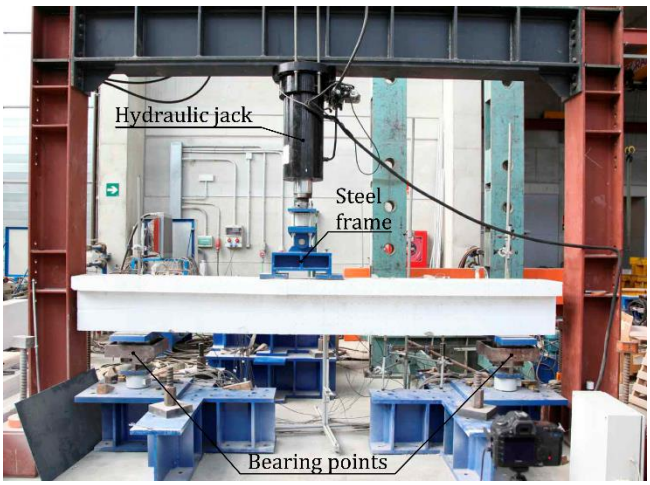

Fig. 6. Experimental setup.

3. Experimental results

3.1. Shear strength and shear-deflection relation

Table 2 shows the vertical shear strength of the test specimens (V_{exp}). The shear-deflection curves of all the test specimens are shown in Fig. 7. Shear force was measured at the principal span. Deflection was measured below the point load located at Section C (LVDT V4 in Fig. 5c). The maximum shear force (V_{exp}) is highlighted with a circle on each curve.

The specimens' self-weight is not included in any shear result since its effect was considered negligible.

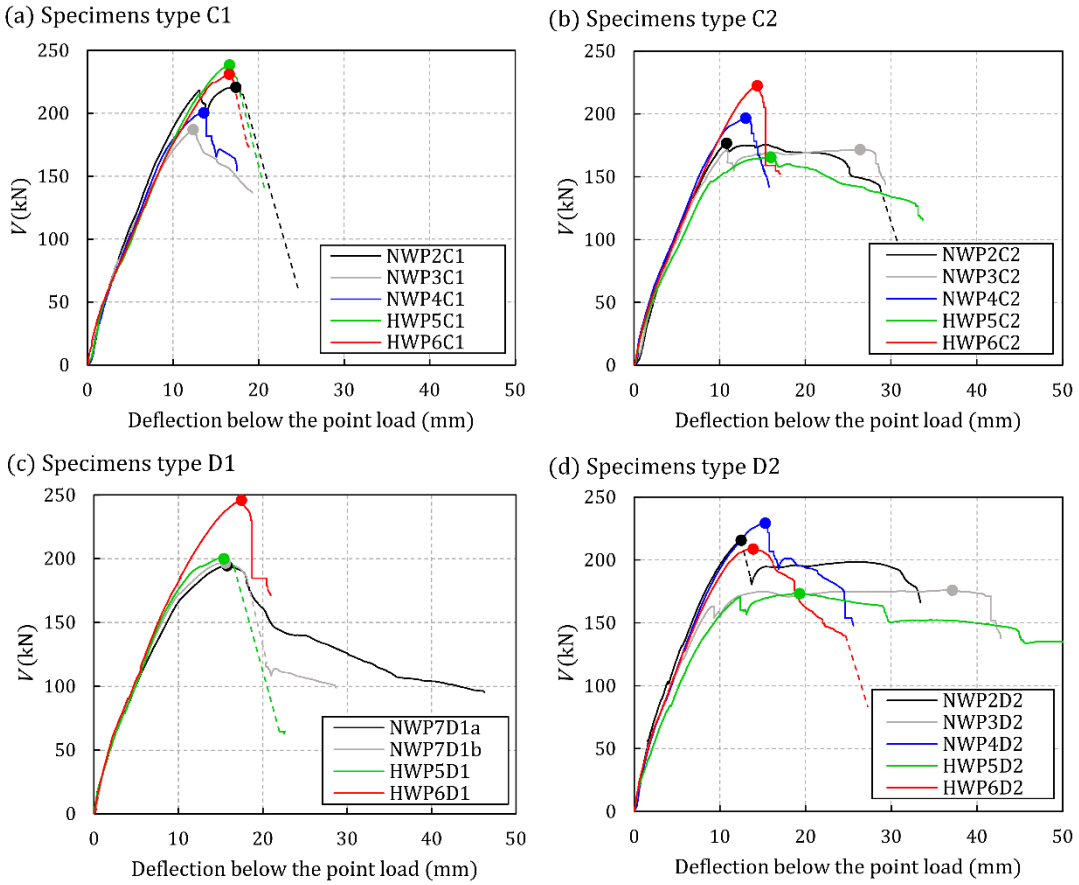

Fig. 7. Shear-deflection relation of the test specimens: (a) specimens with section type C1; (b) specimens with section type C2; (c) specimens with section type D1; (d) specimens with section type D2.

3.2. Crack patterns

Fig. 8 shows the principal span crack patterns of the test specimens in different load stages: at maximum shear force V_{exp}; immediately after V_{exp}, when some sudden cracks appeared, which were normally accompanied by a load drop (e.g., see specimen HWP6C2 in Fig. 7b); at the end of testing.

Fig. 8. Crack patterns of the test specimens in different test stages.

In all the test specimens, vertical bending cracks at the bottom of the principal span appeared in the first load stages. While the cracks in the area below the point load remained vertical, some of the bending cracks at the shear span changed direction towards the point

load as load increased, and formed the diagonal cracks, as observed in previous shear studies [1,2,25,29].

When diagonal cracks approached the plane in which the section width changed, in both the monolithic and composite specimens they deviated along this weakness plane (interface from now on) instead of penetrating the beam's head (slab from now on to refer to the flanges of the monolithic beams and the slab of the composite beams). This horizontal cracking at the flange-web interface (interface crack) has also been observed in multiple experimental studies on monolithic T-shaped beams with web reinforcement found in the literature [25,26,29,48], and also in composite T-shaped specimens with web reinforcement [2,6,10].

In most monolithic specimens, the diagonal cracks at the web were concentrated near the load (e.g., see specimen NWP3C1 in Fig. 8). In specimens C1 and D1, the interface crack extended from the loading plate to stirrups w3 or w4 (see Fig. 5a). Only in specimen HWP6D1 did this interface crack extend to a closer section to the support, stirrup w2, after the maximum load was reached (see Fig. 8). At the maximum load, V_{exp}, the slab of the monolithic specimens, remained mostly undamaged (except for that of specimens NWP4C1 and HWP5D1, where a diagonal crack had already penetrated the slab at V_{exp}). After V_{exp}, a diagonal crack ran through the slab towards the point load. Only in three of the nine monolithic specimens (NWP3C1, NWP7D1a and HWP6D1) did the slab show a different cracking pattern, in which a horizontal splitting crack appeared at the slab's longitudinal reinforcement level after the maximum load. The formation of the slab cracks was generally accompanied by the formation of horizontal cracks at the tension longitudinal reinforcement level [27,35].

In the composite specimens, web diagonal cracks were more distributed along the shear span than in the monolithic specimens (e.g., see specimen NWP3C2). The interface crack was also more extended and reached stirrup w2 in many specimens (see Fig. 5a) at V_{exp}

(specimens NWP2C2, NWP3C2, NWP3D2 and HWP5D2). In other specimens, the interface crack extended to stirrup w2 after V_{exp} (NWP2D2, NWP4D2 and HWP6D2). The slab showed some bending cracks in all these specimens, which started at top of the area close to the end of interface cracking (see NWP3D2 at Fig. 8), and some horizontal cracks appeared at the slab long after the maximum load had occurred (see NWP2C2 in Fig. 8). In other composite specimens, the interface crack extended only to stirrup w3 (NWP4C2 and HWP5C2) or w4 (HWP6C2). In these specimens, a diagonal crack developed in the slab after V_{exp}, as observed in Fig. 8, also with the formation of horizontal cracks at the tension longitudinal reinforcement level.

3.3. Instrumentation results

The main results of the strain gauges located on the steel bars at V_{exp} were analysed. The strain gauges located at the mid-length of the two legs of instrumented stirrups w3 to w5 (see Fig. 5a) measured strains at V_{exp} which exceeded the steel yield strain in tension in all cases, which was 2.7‰ according to Table 3. The average strains of the two strain gauges located on stirrup w6 (Fig. 5a) were lower: 1.6‰ in tension on average for all the tested specimens. The average strain of the two strain gauges located on the bottom layer of the tension longitudinal reinforcement below the point load (gauges G5 and G6 in Fig. 5a) was generally below the steel yield strain (see Table 3), and gave 2.3‰ in tension on average for all the specimens. This confirmed that specimens were far from the bending failure at V_{exp}.

Fig. 9 shows the strains measured in four specimens, on one example for each cross-section type (see Fig. 2), by the strain gauges located on top of the slab: gauges C1, C2 and C3 at Section A and gauges C4, C5 and C6 at Section B (see Fig. 5a).

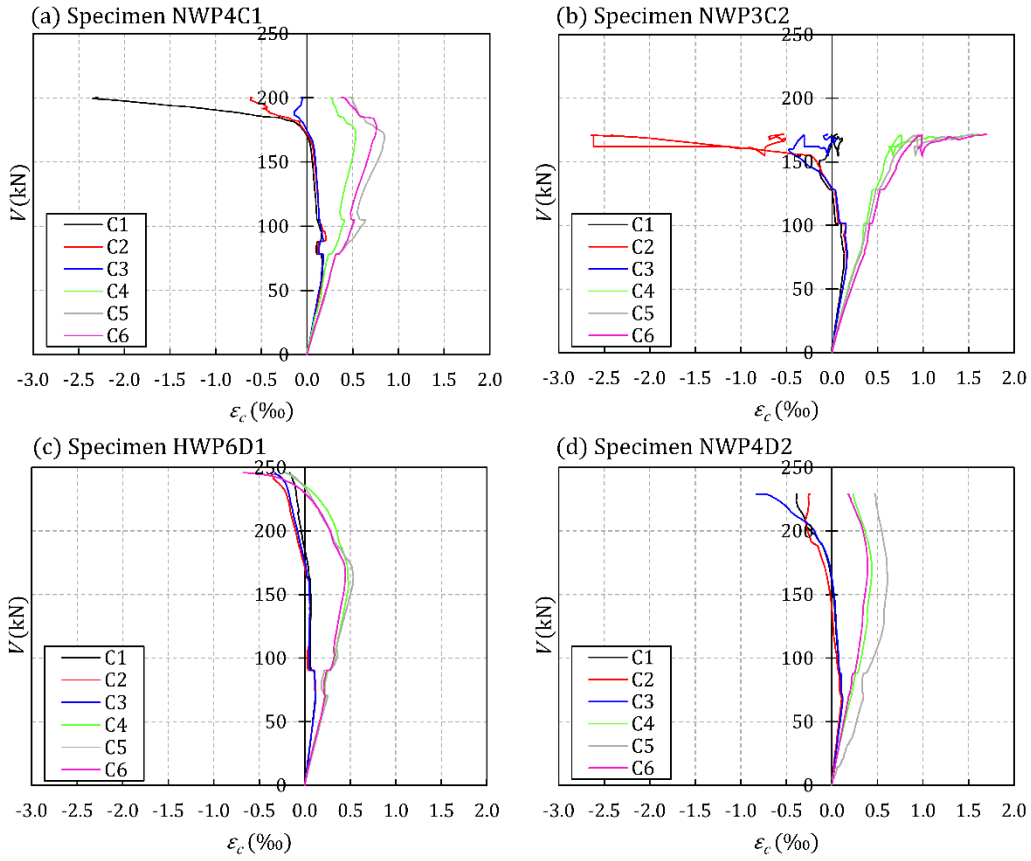

Fig. 9. Results of the strain gauges located on concrete's surface on top of the slab for different specimens: (a) specimen NWP4C1; (b) specimen NWP3C2; (c) specimen HWP6D1; (d) specimen NWP4D2 (positive ε_c for compression).

4. Analysis and discussion

4.1. Analysis of the shear strength mechanism

4.1.1. Shear strength mechanism description

Based on the observations of the crack patterns and the measurements of the strain gauges, the shear transfer actions (STAs) governing specimens' behaviour until the first diagonal cracks formed were identical in both the monolithic and composite beams, and the same as those observed in the rectangular beams studied in [24]: the combined action of the aggregate interlock in cracks, the cantilever action between cracks, the dowel action of the longitudinal reinforcement, the residual tensile strength of concrete and arching action [36,39]. After the diagonal cracks had formed, tensile forces developed in the shear reinforcement.

With increasing load, diagonal cracks continued to reach the plane where the section width changes and developed along this plane instead of penetrating the beam's head, because this was the weakest section in both the monolithic and composite beams. This behaviour was also observed in the rectangular composite specimens in [24]. Thus the shear strength mechanism was similar to that described in [24], in which this horizontal crack divided the shear transfer mechanisms into two paths: one through the beam's web (or the precast beam in the composite specimens) and one through the beam's head (or the slab in the composite beams). The shear transfer mechanism through the precast beam can be explained by a strut-and-tie model composed of two superimposed trusses (coloured in blue in Fig. 10). The shear transfer mechanism through the slab can be considered that of a member without shear reinforcement and modelled with a simple strut-and-tie model (coloured in green in Fig. 10), where transverse ties represent concrete in tension. Both shear transfer mechanisms are connected through the interface crack, where the dowel action of web reinforcement and aggregate interlock actions can take place. The connection between both triangulated bar structures is made by means of finite-dimensional nodes, in which only horizontal forces are considered to act. A more detailed explanation of this model is found in Appendix B.

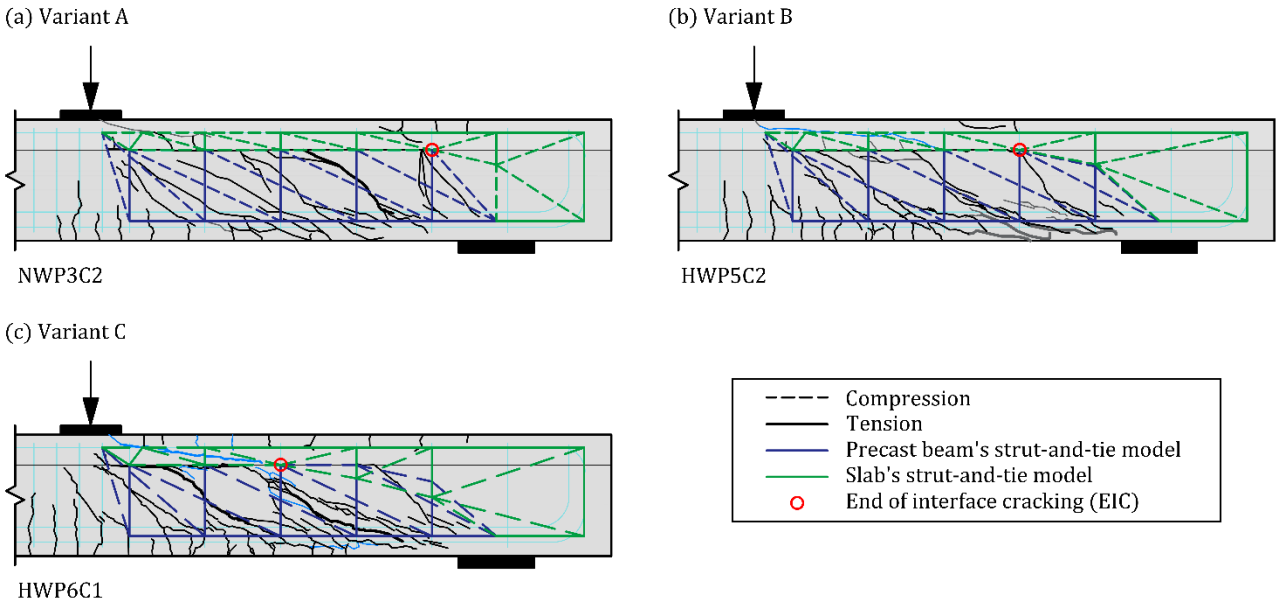

Fig. 10. Strut-and-tie model for the precast beam and the cast-in-place slab proposed in [24]: (a) Variant A (specimen NWP3C2); (b) Variant B (specimen HWP5C2); (c) Variant C (specimen HWP6C1).

The different beam web and slab widths result in a three-dimensional stress distribution in the slab. This was verified in the experimental tests by comparing the measures of the three strain gauges C1, C2 and C3 at Section A and C4, C5 and C6 at Section B (Fig. 5). As shown in Fig. 9, the strain measured by the central gauge did not significantly differ from that measured by the gauges at the flange ends. This meant that the effective width of the compression block in the slab equalled the total slab width in both the type C and D series. Note that high tensile strains for loads close to failure were recorded for some gauges (C1 in Fig. 9a and C2 in Fig. 9b), which were consistent with the cracks observed at the top slab side around Section A.

Similarly to the rectangular composite beams with interface cracking, which were analysed by the authors in [24], the three variants of the proposed model in [24] (Variants A, B and C) can be identified in the beams of this experimental programme depending on interface crack length (see the examples of Fig. 10 for each variant). For sake of clarity, the point of the interface closest to the support where the interface crack ended (EIC) is marked. Table 4 shows the variant of the model that was attributed to each specimen. These were attributed according to the observed crack pattern. The measurements of the strain gauges

1 located on the slab also indicated signs of the variant of the mechanical model adopted by
2 specimens. For example, in the specimens showing a shear strength mechanism like that of
3 Variant A, the strain gauges located at Section B (C4, C5 and C6 in Fig. 5a) showed a tendency
4 towards compression throughout the test (see Fig. 9b) in accordance with the struts
5 represented in the strut-and-tie model of the slab at that section (see Fig. B.1a). On the
6 contrary in the specimens with Variant C, these gauges displayed a tension tendency about
7 halfway through the test (see Fig. 9a, c and d), which proved that strain gauges were close
8 to a tensile zone in concrete, as represented in the strut-and-tie model of Variant C (see Fig.
9 B.1c).

10 *Table 4. Estimated shear strength values of test specimens according to the extension of the model proposed in*
11 *[24] to T-shaped specimens.*

Specimen	Variant	Experimental failure mode	V_{exp} (kN)	V_{pb} (kN)	$V_{s,BF}$ (kN)	$V_{s,SF}$ (kN)	$V_{s,IF}$	V_{pred} (kN)	Predicted failure mode	V_{exp}/V_{pred}
NWP2C1	C	SF	221	108	152	104	-	212	SF	1.04
NWP3C1	C	SF	187	108	152	95	-	203	SF	0.92
NWP4C1	C	SF	200	108	152	109	-	218	SF	0.92
HWP5C1	C	SF	238	108	147	104	-	212	SF	1.12
HWP6C1	C	SF	231	108	149	126	-	235	SF	0.99
NWP7D1a	B	SF	195	108	84	71	-	179	SF	1.09
NWP7D1b	B	SF	197	108	84	71	-	179	SF	1.10
HWP5D1	C	SF	200	108	147	104	-	212	SF	0.94
HWP6D1	C	SF	246	108	149	126	-	234	SF	1.05
NWP2C2	A	BF	177	108	61	100	106	169	BF	1.05
NWP3C2	A	BF	172	108	61	111	106	169	BF	1.02
NWP4C2	B	SF	197	108	87	100	106	195	BF	1.01
HWP5C2	B	SF	166	108	83	68	106	176	SF	0.94
HWP6C2	C	SF	222	108	148	107	106	216	IF	1.03
NWP2D2	C	IF	216	108	152	102	106	210	SF	1.03
NWP3D2	A	BF	176	108	61	112	106	169	BF	1.04
NWP4D2	C	IF	229	108	152	94	106	202	SF	1.13
HWP5D2	A	BF	173	108	59	66	106	167	BF	1.04
HWP6D2	C	IF	209	108	148	107	106	216	IF	0.97

12 ### *4.1.2. Failure modes*

13 According to the above-described shear strength mechanism, the ultimate load of a T-beam
14 with an interface crack is the sum of the shear resisted by the precast beam (given by the
15 strut-and-tie model by considering that all stirrups had reached their yielding strength, as
16 proved experimentally by the measurements of the stirrups' strain gauges at Section 3.3)

and the shear strength transferred by the slab at failure. As the maximum shear resisted by the precast beam was reached before slab failure and it remained constant for increasing loads until the slab failed, the specimen's shear strength was reached when the slab failed. Depending on the interface crack length, three failure modes can occur in the slab or at the interface: slab bending failure (BF); slab shear failure (SF); interface failure (IF).

4.1.2.1. Slab bending failure (BF in Table 4)

This failure mode was identified in the specimens where a long interface crack was developed (Variant A in Fig. 10). The specimens that exhibited this failure mode showed shear-strain curves (Fig. 7) with no marked drop upon the maximum load. In addition, vertical cracks were observed on the upper slab side (e.g., see NWP3C2 in Fig. 8) and tensile strains were measured in the slab strain gauges above the point EIC in Fig. 10 (see gauges C1, C2 and C3 in Fig. 9b). This denotes the existence of a negative bending moment resisted by the slab in this area.

4.1.2.2. Slab shear failure (SF in Table 4)

This failure mode was observed in some composite specimens and in all the monolithic specimens of this experimental programme. Upon maximum shear, a diagonal crack in the slab developed in direction to the point load (e.g., see NWP2C1 in Fig. 8) and, thus, a pronounced load drop in the shear-deflection curves took place (Fig. 7). This failure mode has also been described in previous studies on monolithic T-shaped beams [25,26,29].

4.1.2.3. Interface failure (IF in Table 4)

Three composite specimens (see NWP2D2, NWP4D2 and HWP6D2 in Fig. 8) showed a cracking pattern with a short interface crack before the peak load took place, that extended towards stirrup w2 (Fig. 5a) afterwards. In these three specimens, and unlike other composite specimens, after the load that led to crack interface extension, no new strength mechanism developed to increase this load. Therefore, the maximum load was determined by the load that produced crack prolongation. This failure mode has not been previously

detected in rectangular composite specimens [24] and is identified in this paper as interface failure (IF).

From the Variant C of the proposed model (see Fig. 10), a new procedure for calculating experimental shear stress at the interface ($\tau_{i,exp}$) was developed (explained in detail in Appendix C). The horizontal shear force ($F_{i,nc}$) at the uncracked interface section was estimated by subtracting the horizontal forces ($F_{H,i}$) transferred through the interface crack from the horizontal force ($S_{H,1}$) resisted by the slab at the loading section (see Fig. C.1 and Appendix C). This shear force was calculated for the three specimens with IF at the load immediately before the interface crack prolonged towards the support (V_{exp}). The uncracked interface length at V_{exp} ($l_{i,nc}$) was known, which was 1.08, 1.18 and 1.02 m for NWP2D2, NWP4D2 and HWP6D2, respectively. Following the procedure described in Appendix C, the mean values of shear stress resistances of the uncracked interface ($\tau_{i,exp}$) were obtained by dividing force $F_{i,nc}$ by the uncracked interface area. The results were respectively 1.97, 2.08 and 1.91 MPa for NWP2D2, NWP4D2 and HWP6D2.

As shown, the shear strength ($\tau_{i,exp}$) of the specimens whose failure mode was described as IF all had a similar value, of around 2.0 MPa and with a minimum value of 1.9 MPa. This value could vary for specimens with different characteristics, such as surface roughness, concrete quality and shear reinforcement.

4.1.3. Estimated shear strength for the specimens of this experimental programme

The component of the shear strength resisted by the precast beam (V_{pb}) could be estimated from the proposed strut-and-tie model by considering that all the vertical ties had reached their yielding strength. This assumption agrees with the measurements recorded at V_{exp} of the strain gauges located at the stirrups (Section 3.3). Stirrup w6 (see Fig. 5a) was the only that was generally less tensioned. However, its yielding was acceptable because this assumption did not significantly affect the result, as proved in a previous study by the

authors [24]. The V_{pb} results for the specimens in this programme are shown in Table 4. The formulation of this model, described in detail in [24], is summarised in Appendix B.

The shear force resisted by the slab when the failure mode was slab bending failure ($V_{s,BF}$) was determined by the slab's ultimate bending moment at the cross-section above point EIC (see Appendix B), and by assuming that all the top longitudinal reinforcement bars reached their yielding strength. The $V_{s,BF}$ results are shown in Table 4.

The shear force resisted by the slab when the failure mode took place by slab shear ($V_{s,SF}$) was estimated by considering that the slab was subjected to a biaxial state of stresses and failure occurred when the concrete's principal stresses reached Kupfer's failure envelope [49]. The vertical shear stresses on the slab are not uniformly distributed along the flange width, but concentrate in the vicinity of the web [50]. In this paper, a shear-effective area of the slab which increased 45º from the cross-section width change was considered in line with previous research [3,38]. Thus to estimate $V_{s,SF}$, the vertical shear stress distribution in the slab was assumed to be uniform at an effective width (b_{eff}), which equalled the sum of web width and flange depth ($b+h_s$), and was parabolic on the slab cross-section, as in other studies found in the literature [33]. As explained later in Section 4.2.1, this assumption was consistent with the experimental results. The $V_{s,SF}$ results are shown in Table 4.

The shear force resisted by the slab when the failure mode was interface shear ($V_{s,IF}$) was estimated by: taking the upper limit of the shear stresses at the interface as being known (1.9 MPa for the specimens of this experimental programme because this was the minimum shear stress obtained); using the equations in Appendix C, where the uncracked interface length at V_{exp} ($l_{i,nc}$) was taken as the horizontal distance between EIC in Variant C (see Fig. 10), located at stirrup w4 (see Fig. 5a), and the end of the beam, which was 1.09 m. The $V_{s,IF}$ results are shown in Table 4.

The slab's shear strength was the minimum value between those obtained for the slab's three failure modes, $V_s = \min(V_{s,BF}, V_{s,SF}, V_{s,IF})$. The value of the three slab resistances that matched this minimum value allowed the model to predict the failure mode.

The specimen's shear strength was obtained by adding the shear forces resisted by the prefabricated beam and the slab ($V_{pred} = V_{pb} + V_s$). The V_{pred} values obtained for the 19 specimens in this experimental programme are found in Table 4. Table 4 also shows the resultant failure mode according to the predicted shear strength values and the experimental to predicted shear strength ratio (V_{exp}/V_{pred}).

From comparing experimentally observed failure mode (third column in Table 4) to the governing failure mode according to the proposed model (tenth column in Table 4), it can be concluded that the model quite well captured the failure mode. Only in a few specimens (NWP4C2, HWP6C2, NWP2C2, NWP4D2) did the predicted failure mode not match that experimentally observed. However in all those specimens, the slab's minimum predicted shear strength value (V_s) came very close to the value predicted for the experimentally observed failure mode.

For all the specimens, the average value and the coefficient of variation of V_{exp}/V_{pred} were respectively 1.02 and 6.07%. These results indicate a good agreement of the shear strength predicted by this model with the experimental results.

4.2. Effect of test parameters on shear strength

4.2.1. Flange width

In this section, the existence of flanges and their width were analysed. To this end, the results of the rectangular cross-section specimens of a previous study by the authors [24], whose geometric and reinforcement characteristics were identical to those of the specimens herein presented, except for the absence of flanges, were employed to make a comparison. Five specimens with monolithic rectangular cross-sections (B1) and six

specimens with composite rectangular cross-sections (B2) from series NW and HW were taken from this study.

Fig. 11 shows the results obtained for the monolithic specimens. By comparing beams B1 and C1, the strengths of the specimens with a flange width that equalled flange depth (C1) increased compared to those of rectangular sections (B1) by an average of 16% for all the fabrication batches. This result comes close to that of around 20-25% observed in the literature for beams with web reinforcement [25,32,33].

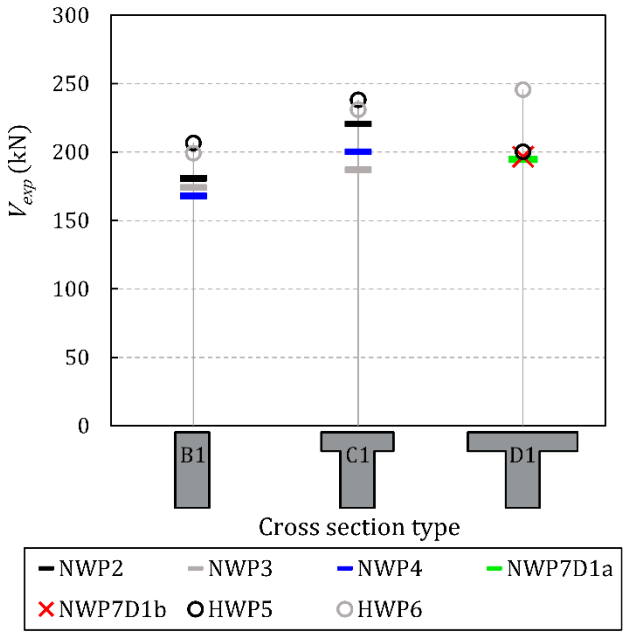

Fig. 11. Comparison of the shear strengths of beams B1, C1 and D1.

Of the D1 specimens, whose flange width was twice flange depth, only the specimens from series HWP5 and HWP6 could be compared. The shear strength of specimen HWP6D1 increased by 23% in relation to specimen HWP6B1 and by 6% in relation to specimen HWP6C1. However, the shear strength of specimen HWP5D1 was less than that of specimens HWP5B1 and HWP5C1. This could be an anomalous result due to a local effect of the applied load.

In Section 4.1.3, a shear-effective area that increased 45º from the cross-section width change [3,38], equal to the web width and flange depth sum, was considered for all the T-shaped specimens with slab shear failure (all the monolithic specimens failed in this way).

This implied a 17% increase in the shear-effective area in relation to that of the rectangular specimens, which agrees the experimental results of specimens C1. As only one D1 specimen could be compared and its shear strength did not significantly increase *versus* specimen C1, the consideration of the same shear-effective area would seem appropriate.

Fig. 12 shows the comparison of the composite specimens. The shear strength of the T-shaped specimens C2, with flange width equalling flange depth, did not increase in most cases in relation to the rectangular specimens B2 of each fabrication batch. The shear strength of the specimens C2 from series NWP2, NWP3, NWP4 and HWP5 decreased 1% on average *versus* B2, while the shear strength of the C2 specimen from series HWP6 increased by 19%.

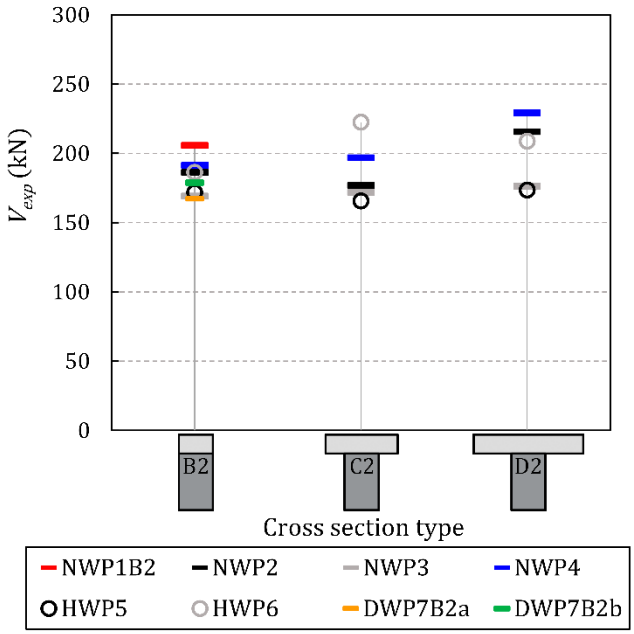

Fig. 12. Comparison among the shear strengths of beams B2, C2 and D2.

Regarding the T-shaped D2 specimens, whose flange width was twice flange depth, the shear strength increased 16% on average for series NWP2, NWP4 and HWP6 in relation to that of the rectangular specimens B2, but this increase was not significant (3% on average) for series NWP3 and HWP5.

These observations of the flange width effect on the composite specimens are consistent with the variants of the mechanical model discussed in Section 4.1. In the specimens with

an extended interface crack, in which the model's Variant A was adopted in most cases (see Table 4), the flange effect was not noticeable because the failure mode (slab bending failure) was explained by the slab's longitudinal reinforcement and not by the slab's shear effective area. Those specimens were those whose shear strength did not significantly differ from that of the rectangular specimens. On the contrary, in the specimens with a limited interface crack (Variant C), shear strength increased compared to specimens B2. Thus slab shear failure was considered to give a good approximation of the experimental shear strength (similar to the value obtained for interface failure) as the shear-effective area of flanges was taken into account (see $V_{s,SF}$ in Table 4).

4.2.2. Presence of an interface between concretes

In order to analyse how the presence of an interface influences shear strength, the beams with the same cross-section geometry and fabricated with one and two concretes were compared. Fig. 13 shows the results for the specimens with sections C1 and C2. When the shear strengths of the beams of the same fabrication batch were compared, the presence of an interface reduced the shear strength of the composite T-beams whose flange width equalled flange depth by 13% on average compared to the monolithic beams.

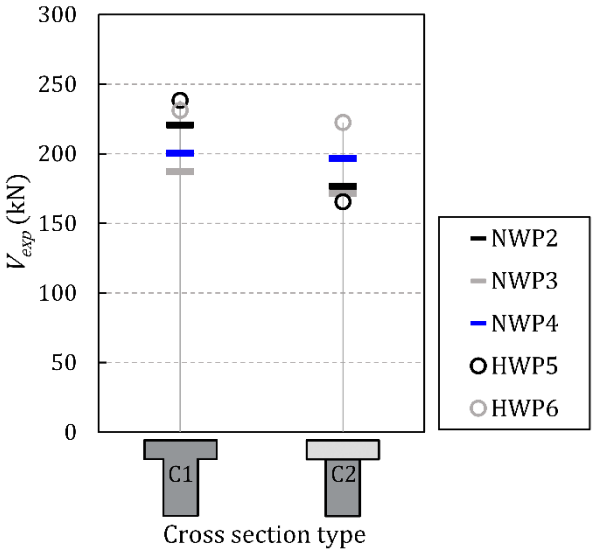

Fig. 13. Comparison between the shear strengths of beams C1 and C2.

Similarly, Fig. 14 shows the results for the specimens with sections D1 and D2. By comparing the beams of the same fabrication batch, the average reduction in shear strength due to the presence of the interface would be 14%.

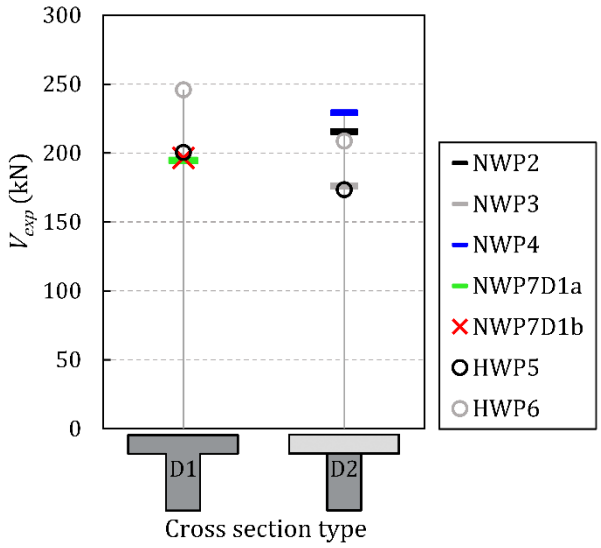

Fig. 14. Comparison between the shear strengths of beams D1 and D2.

The lower strength of the composite specimens *versus* the monolithic ones can be explained by the shear strength mechanisms described in Section 4.1.1. An interface existing between concretes causes a higher extension of the interface crack, which can bring about weaker shear strength mechanisms, like that of Variant A (Fig. 10), with less resistant failure modes, like BF or IF (see Table 4). The monolithic specimens presented stronger shear strength mechanisms, like Variant C or B, which brought about the higher shear strengths provided by slab shear failure (SF in Table 4).

4.2.3. Strength of the concrete in beam and slab

When comparing the monolithic specimens of series NW fabricated with NSC, and HW fabricated with HCS, the better-quality concrete increased shear strength by 15% on average. This concrete strength effect was considered in the proposed model in Section 4.1 as the shear strength of the monolithic specimens was estimated from slab shear failure, in which the concrete strength of the beam's head is a variable of the formulation (see Appendix B).

Regarding the composite specimens, the shear transfer mechanism described in Section 4.1 also allowed the experimental results to be explained.

For the composite specimens failing by slab bending failure (BF) (specimens NWP2C2, NWP3C2, NWP4C2 and HWP5D2 in Table 4), the experimental shear strengths were similar (177, 172, 176 and 173 kN, respectively). This is consistent with the assumption that in this failure mode, the beam's shear reinforcement and the slab's longitudinal reinforcement reached their yielding strength.

When comparing composite specimens NWP4C2 and HWP5C2, whose failure was caused by slab shear failure, and both with similar interface crack length, shear strength significantly varied (197 and 166 kN, respectively, in Table 4). This demonstrates that shear strength depended directly on the compressive strength of the slab's concrete (33 and 22 MPa, respectively).

In the specimens with interface failure (IF in Table 4), no significant variations were observed in the shear strength with the compressive strength of both the beam and slab's concretes, but with the beam concrete's workability during casting. This was also observed by the authors in a previous study [24]. The specimens with drier concretes in the beam (see the slump measurements in Table 2), such as specimens NWP2D2 and NWP4D2, exhibited higher as-cast interface roughness and, therefore, higher interface shear strength. This resulted in slightly higher shear strength than in those specimens with more fluid concretes (HWP6D2). However, the compressive strength of the beam's concrete in the latter was higher.

4.3. Comparison of the test results with existing code provisions and the proposed model

The test specimens' shear strength was assessed with the shear formulations for elements with web reinforcement according to current design codes EC2 [21], MC-10 [22] at its three

approximation levels, and the two equations of ACI 318-19 [23] (named (a) and (b) in Section 22.5.5.1 of ACI 318-19). As no code accounts for the flanges effect on shear strength, only the web of specimens was considered. In the composite specimens, different shear area considerations were included: only the precast beam resisted shear, in which case the precast beam's effective depth (d_b) and the compressive strength of the beam's concrete ($f_{c,b}$) were used in the formulations; or the entire composite beam's web resisted shear, in which case the composite beam effective depth (d_c) and the compressive strength of the beam's concrete ($f_{c,b}$), the slab's concrete ($f_{c,s}$) or the weighted average of the compressive strengths of both concretes ($f_{c,wa}$) were used [1,4,24]. The mean value and the coefficient of variation (CV) of the experimental shear strength (V_{exp}) to the predicted value (V_{pred}) ratio are shown in Table 5. These statistical indicators were used to analyse the studied sample, although more elements in the sample would be necessary for the values of these indicators to be significant. Note that the specimens with similar concrete compressive beam and slab strengths (series NW) were assessed only with $f_{c,wa}$ when d_c was considered as the results were similar. The tested average values of the materials were used with all the formulations, and the partial safety factors for the concrete (γ_c) and steel material properties (γ_s) were 1.0. No formulation for any specimen offered unsafe results.

Table 5. Statistical indicators of the V_{exp}/V_{pred} ratio for the test specimens assessed with current codes formulations.

Specimens	No. of specimens	Method	EC2		MC-10 LI		MC-10 LII		MC-10 LIII		ACI 318-19 (a)		ACI 318-19 (b)	
			Mean	CV (%)	Mean	CV (%)	Mean	CV (%)	Mean	CV (%)	Mean	CV (%)	Mean	CV (%)
Monolithic	9	d_b, $f_{c,b}$	1.31	9.53	1.89	9.53	1.67	9.53	1.35	7.03	1.59	6.14	1.36	6.01
Composite (NW)	6	d_b, $f_{c,b}$	1.70	11.19	2.46	11.19	2.14	11.19	1.75	10.25	2.09	9.70	1.67	9.37
		d_c, $f_{c,wa}$	1.19	11.19	1.72	11.19	1.52	11.19	1.24	10.62	1.47	10.26	1.25	10.11
Composite (HW)	4	d_b, $f_{c,b}$	1.69	12.33	2.44	12.33	2.12	12.33	1.66	11.04	1.94	10.18	1.53	9.71
		d_c, $f_{c,b}$	1.18	12.33	1.71	12.33	1.51	12.33	1.18	11.06	1.36	10.18	1.15	9.84
		d_c, $f_{c,s}$	1.18	12.33	1.71	12.33	1.51	12.33	1.28	8.50	1.53	7.14	1.32	6.21
		d_c, $f_{c,wa}$	1.18	12.33	1.71	12.33	1.51	12.33	1.20	10.72	1.39	9.63	1.18	9.18

For the monolithic specimens, the code that better approached the experimental results was EC2, with a mean value of 1.31 and a low CV (see Table 5). Equation (b) of ACI 318-19 and Level III of MC-10 gave a similar result. When comparing these results to those for the

rectangular specimens of [24], which were more accurate, all the formulations can be considered to be very much on the safety side as the flange effect was not taken into account.

For the composite specimens, the shear strengths predicted by considering that only the precast beam resisted shear were extremely safe with all the codes. When considering the entire composite beam's effective depth in series NW, EC2 gave the most accurate result (mean value of 1.19). For series HW, EC2, MC-10 LI and MC-10 LII obtained the same results for all the perspectives as the calculation did not depend on the concrete compressive strength for these test specimens. The best result was provided by equation (b) of ACI 318-19 when using $f_{c,b}$ (mean value of 1.15) due to the higher compressive strength of the beam's concrete. Despite this good result, we should bear in mind that using $f_{c,b}$ is commonplace for calculating shear strength [16,19], but can lead to unsafe results if the beam's depth value is not much higher than that of the slab, as observed in [5]. In this case, using $f_{c,wa}$ would be a safer practical solution for which EC2, MC-10 LIII and ACI 318-19 gave very good estimations.

The formulation described in Section 4.1 was also used to assess specimens' shear strengths. As the interface crack extension is unknown prior to testing, the weakest shear strength mechanisms observed in the experimental tests were considered. Thus the monolithic specimens were considered to resist shear by means of the Variant B of the strut-and-tie model (Fig. 10) and slab shear failure. The composite specimens were calculated with Variant A of the strut-and-tie model and slab bending failure. The results are shown in Table 6.

Table 6. Statistical indicators of the V_{exp}/V_{pred} ratio for the test specimens assessed with the proposed model.

	Monolithic	Composite (NW)	Composite (HW)
No. of specimens	9	6	4
Mean	1.03	1.15	1.15
CV (%)	7.55	11.19	12.11
Min. value	0.92	1.02	0.99
Max. value	1.15	1.36	1.33
No. of unsafe results	4	0	1

The proposed model gave a very good approximation to the monolithic specimens' actual strength (mean value of 1.03 and CV of 7.55%), albeit with some unsafe results. The composite specimens were well estimated by this methodology, whose good result was similar to the best one offered by the codes and with almost no unsafe results. The obtained dispersions were similar to those observed in Table 5. It should be noted that the model is based on a composite beam mechanical model supported by experimental results, and was developed for the shear strength assessment of the specimens included in this experimental programme. Further experimental research should be conducted to extend the application scope of this mechanical model.

5. Recommendations for practice

After performing the experimental tests, analysing the shear strength mechanisms and the influence of the considered variables, adapting the strut-and-tie model to these specimens and experimentally verifying the current codes' formulations and the proposed one, some preliminary practical rules for designing this type of composite elements were derived.

For increasing the shear strength of the composite structure, the most resistant observed mechanisms must be sought, which were the Variant C of the model with a slab shear failure. For the specimen to develop these mechanisms, the interface shear strength must be increased, by increasing the interface roughness or the reinforcement crossing the interface.

If the interface shear strength is improved, there are other measures that can increase the composite element's shear strength. First, the widening of the slab. The specimens tested in this paper proved the flanges can increase the specimen's shear strength when a slab shear failure takes place. The flange width that contributes to shear strength would be limited to once the flange depth, according to these experimental results. Second, the use of a better-quality concrete at the slab, since it increases the slab shear strength.

If the interface shear strength cannot be improved, the shear strength of the composite element can be safely estimated by the sum of the precast beam shear strength and the shear strength of the slab given by the yielding of the slab's longitudinal reinforcement (see the formulation presented in Appendix B).

It must be taken into account that the results and the discussion of this experimental analysis were derived from the tested specimens' dimensions, reinforcement and concrete quality. A generalization of the proposed lower-bound plasticity-based model to specimens of other characteristics will be needed in the future to better elaborate these practical rules.

6. Conclusions

The main findings of this study on the shear strength of concrete composite beams with T-shaped cross-section and web reinforcement are:

1. The plane in which the section width changes (interface) is a weakness plane in which interface cracks develop. These interface cracks divide the shear transmission into two load paths in both the monolithic and composite beams: one through the precast beam; one through the cast-in-place slab. The total shear strength of a specimen can be considered to be the sum of the shear forces transmitted by each path. Ultimate shear is given by three possible failure modes in the slab: bending failure, shear failure and interface failure.
2. The mechanical model proposed in a previous study by the authors [24], which is adapted to the monolithic and composite T-shaped specimens of this paper, proved useful for understanding both the shear transfer mechanisms and failure modes of the experimental tests run in this work. The model accounts for the effect of flanges. Besides, the formulation of a failure mode detected in this paper (interface failure) is herein developed.

3. In the specimens with slab shear failure (all the monolithic specimens and some composite specimens), the presence of flanges increased shear strength. In this research work specimens, the shear strength increased in the same proportion as the shear-effective area increases when considering an effective slab width that equal the sum of the web width and flange depth (approx. 17%). Most of the specimens with extended interface cracking, which were composite specimens in this test programme, showed slab bending failure, and flanges did not increase shear strength.
4. The presence of an interface between concretes decreased the specimens' shear strength, since the greater interface cracking resulted in less resistant failure mechanisms, such as slab bending failure in the beams with extended interface cracking.
5. The shear strength of the tested specimens that presented an extended interface cracking did not depend on the compressive strength of either the beam or slab's concrete, since, according to the proposed model, their shear strength is given by the yielding of the slab's longitudinal reinforcement. The shear strength of the specimens in which interface cracking was short depended on the compressive strength of the slab's concrete, since the shear strength is given by the slab failing in shear.
6. When predicting the monolithic specimens' shear strength with the current codes formulations, EC2 [21] gives the best result, but still extremely safe as no code accounts for the flanges effect on shear strength. Regarding the composite specimens, EC2, the level III approximation of MC-10 [22] and equation (b) of ACI 318-19 [23], using the weighted average of the beam and slab's concrete compressive strengths, offer the best estimations, on the safety side. Predicting the monolithic specimens' shear strength with the proposed model gives very accurate results. The shear strength estimation performed with the proposed model for the composite specimens is also good, and slightly better than that of the current codes.
7. As a recommendation for practice, the improvement of the interface shear strength of composite beams is suggested for increasing their shear strength. This will derive in the

specimen having a slab shear failure. In this case, the slab width and the slab's concrete strength could be increased with the same purpose. If the interface shear strength cannot be improved, the composite specimen's shear strength can be safely predicted with the proposed model for beams with extended interface cracking.

This research work contributes to increase the number of experimental tests on concrete composite elements subjected to shear forces. Experimental data on the contribution of the cast-in-place slab to shear strength and a better understanding of shear strength mechanisms in concrete composite T-beams are provided. The mechanical model proposed to explain the experimental results could be used as a reference to develop a shear strength predictive model for concrete composite beams in the future. However, to delve into the slab's contribution to shear strength, further research should be conducted on more complex elements, such as T- or I-shaped beams with a cast-in-place slab on top and of different dimensions.

Acknowledgements

The authors would like to thank the Ministerio de Ciencia e Innovación (MCIN) and the Agencia Estatal de Investigación (AEI) for their support through grants BIA2015-64672-C4-4-R and RTI2018-099091-B-C21-AR, both funded by MCIN/AEI/ 10.13039/501100011033 and by "ERDF A way of making Europe". Author Lisbel Rueda-García was supported through grant BES-2016-078010 funded by MCIN/AEI/ 10.13039/501100011033 and by "ESF Investing in your future". The Regional Government of Valencia also supported this research through Project AICO/2018/250. This research work was undertaken at the Concrete Science and Technology University Institute (ICITECH) of the Universitat Politècnica de València (UPV; Spain) with concrete supplied by Caplansa.

References

[1] Kim C-G, Park H-G, Hong G-H, Kang S-M, Lee H. Shear Strength of Concrete Composite Beams with Shear Reinforcements. ACI Struct J 2017;114:827–37.

[2] Halicka A, Jabłoński Ł. Shear failure mechanism of composite concrete T-shaped beams. Proc Inst Civ Eng Struct Build 2016;169:67–75.

[3] Ribas González CR, Fernández Ruiz M. Influence of flanges on the shear-carrying capacity of reinforced concrete beams without web reinforcement. Struct Concr 2017. https://doi.org/10.1002/suco.201600172.

[4] Kim C-G, Park H-G, Hong G-H, Kang S-M. Shear strength of composite beams with dual concrete strengths. ACI Struct J 2016;113:263–74.

[5] Rueda-García L, Bonet JL, Miguel Sosa PF, Fernández Prada MÁ. Safety assessment of shear strength current formulations for composite concrete beams without web reinforcement. In: Fédération Internationale du Béton (fib), editor. Proc. 2021 fib Symp. Concr. Struct. New Trends Eco-Efficiency Perform., Lisbon: 2021, p. 2305–14.

[6] Loov RE, Patnaik AK. Horizontal Shear Strength of Composite Concrete Beams With a Rough Interface. PCI J 1994;39:48–69.

[7] Saemann JC, Washa GW. Horizontal Shear Connections between Precast Beams and Cast-in-Place Slabs. ACI J Proc 1964;61:1383–409.

[8] Kahn LF, Slapkus A. Interface Shear in High Strength Composite T-Beams. PCI J 2004;49:102–10.

[9] Kovach J, Naito C. Horizontal Shear Capacity of Composite Concrete Beams without Interface Ties. ATLSS Report No. 05-09: 2008.

[10] Tan KH, Guan LW, Lu X, Lim TY. Horizontal shear strength of indirectly loaded composite concrete beams. ACI Struct J 1999;96:533–8.

[11] Fang Z, Jiang H, Liu A, Feng J, Chen Y. Horizontal Shear Behaviors of Normal Weight and Lightweight Concrete Composite T-Beams. Int J Concr Struct Mater 2018;12. https://doi.org/10.1186/s40069-018-0274-3.

[12] Hartmann DL, Breen JE, Kreger ME. Shear capacity of high strength prestressed concrete girders. Austin: 1988.

[13] Shahawy MA, Batchelor B deV. Shear Behavior of Full-Scale Prestressed Concrete Girders: Comparison Between AASHTO Specifications and LRFD Code. PCI J 1996;41:48–62. https://doi.org/10.15554/pcij.05011996.48.62.

[14] Ross BE, Ansley MH, Hamilton III HR. Load testing of 30-year-old AASHTO Type III highway bridge girders. PCI J 2011;56.

[15] Hamilton III HR, Llanos G, Ross BE. Shear performance of existing prestressed concrete bridge girders. 2009.

[16] Runzell B, Shield C, French C. Shear Capacity of Prestressed Concrete Beams. 2007.

[17] Cumming, A David., Shield, Carol K., French CE. Shear Capacity of High-Strength Concrete Pre-stressed Girders. 1998.

[18] Hawkins NM, Kuchma DA. Application of LRFD Bridge Design Specifications to High-Strength Structural Concrete: Shear Provisions. 2007.

[19] Avendaño AR, Bayrak O. Shear strength and behaviour of prestressed concrete beams. Technical Report: IAC-88-5DD1A003-3, Texas Department of Transportation: 2008.

[20] Ruiz MF, Muttoni A. Shear strength of thin-webbed post tensioned beams. ACI Struct J 2009;106.

[21] CEN. EN 1992-1-1:2004. Eurocode 2: Design of concrete structures - Part 1-1: General rules and rules for buildings. 2004.

[22] Fédération International du Béton (fib). Model Code 2010. Ernst & Sohn; 2012.

[23] ACI Committee 318. Building code requirements for structural concrete (ACI 318-19); and commentary (ACI 318R-19). Farmington Hills: American Concrete Institute; 2019.

[24] Rueda-García L, Bonet Senach JL, Miguel Sosa PF, Fernández Prada MÁ. Analysis of the shear strength mechanism of slender precast concrete beams with cast-in-place slab and web reinforcement. Eng Struct 2021;246:113043. https://doi.org/10.1016/j.engstruct.2021.113043.

[25] Placas A. Shear failure of reinforced concrete beams. Faculty of Engineering of the University of London. Imperial College of Science and Technology, 1969.

[26] Giaccio C, Al-Mahaidi R, Taplin G. Experimental study on the effect of flange geometry on the shear strength of reinforced concrete T-beams subjected to concentrated loads. Can J Civ Eng 2002;29. https://doi.org/10.1139/l02-099.

[27] Zararis IP, Karaveziroglou MK, Zararis PD. Shear strength of reinforced concrete T-beams. ACI Struct J 2006;103:693–700.

[28] Kani MW, Mark W. Huggins, Rudi R. Wittkopp. Kani on shear in reinforced concrete. Toronto: University of Toronto, Dept. of Civil Engineering; 1979.

[29] Palaskas MN, Attiogbe EK, Darwin D. Shear strength of lightly reinforced T-beams. J Am Concr Inst 1981;78:447–55.

[30] Tureyen AK, Wolf TS, Frosch RJ. Shear strength of reinforced concrete T-beams without transverse reinforcement. ACI Struct J 2006;103.

[31] Ayensa A, Oller E, Beltrán B, Ibarz E, Marí A, Gracia L. Influence of the flanges width and thickness on the shear strength of reinforced concrete beams with T-shaped cross section. Eng Struct 2019;188:506–18.

https://doi.org/10.1016/j.engstruct.2019.03.057.

[32] ACI/ASCE Task Committee 426. The shear strength of reinforced concrete members. ACI J 1973;99:1091–187.

[33] Cladera A, Marí A, Ribas C, Bairán J, Oller E. Predicting the shear-flexural strength of slender reinforced concrete T and I shaped beams. Eng Struct 2015;101. https://doi.org/10.1016/j.engstruct.2015.07.025.

[34] Swamy RN, Qureshi SA. An ultimate shear strength theory for reinforced concrete T-beams without web reinforcement. Matériaux Constr 1974;7:181–9. https://doi.org/10.1007/BF02473833.

[35] Leonhardt F, Walther R. Schubversuche an einfeldrigen Stahlbetonbalken mit und ohne Schubbewehrung zur Ermittlung der Schubtragfähigkeit und der oberen Schubspannungsgrenze. Heft 151. Berlin: Ernst & Sohn; 1962.

[36] Placas A, Regan PE, Baker ALL. Shear failure of reinforced concrete beams. J Amer Concr Inst 1971;68.

[37] Regan MM and PE. Shear Strength of Prestressed and Reinforced Concrete T-Beams. ACI Symp Publ 1974;42. https://doi.org/10.14359/17284.

[38] Ribas C, Cladera A, Mas B. Modelo cortante-flexión para el dimensionamiento a ELU de forjados de vigueta pretensada y bovedilla. VI Congr. Int. Estructuras ACHE, Madrid, Spain: 2014, p. 151–152.

[39] Fernández Ruiz M, Muttoni A, Sagaseta J. Shear strength of concrete members without transverse reinforcement: A mechanical approach to consistently account for size and strain effects. Eng Struct 2015;99:360–72. https://doi.org/10.1016/j.engstruct.2015.05.007.

[40] Rueda-García L, Bonet Senach JL, Miguel Sosa PF. Experimental study of concrete

composite beams subjected to shear. Proc. fib Symp. 2019 Concr. - Innov. Mater. Des. Struct., 2019, p. 1779–86.

[41] UNE-EN 12350-2:2020. Testing fresh concrete - Part 2: Slump test. 2020.

[42] UNE-EN 12390-3:2020. Testing hardened concrete - Part 3: Compressive strength of test specimens. 2020.

[43] UNE-EN 12390-6:2010. Testing hardened concrete - Part 6: Tensile splitting strength of test specimens. 2010.

[44] UNE-EN 12390-13:2014. Testing hardened concrete - Part 13: Determination of secant modulus of elasticity in compression. 2014.

[45] Comisión Permanente del Hormigón. EHE-2008. Instrucción de Hormigón Estructural. Ministerio de Fomento. Madrid: 2008.

[46] UNE-EN ISO 6892-1:2017. Metallic materials - Tensile testing - Part 1: Method of test at room temperature. 2017.

[47] Rueda-García L, Bonet Senach JL, Miguel Sosa PF, Fernández Prada MÁ. Experimental analysis of the shear strength of composite concrete beams without web reinforcement. Eng Struct 2021;229:111664. https://doi.org/10.1016/j.engstruct.2020.111664.

[48] Pansuk W, Sato Y. Shear mechanism of reinforced concrete T-Beams with stirrups. J Adv Concr Technol 2007;5. https://doi.org/10.3151/jact.5.395.

[49] Kupfer HB, Gerstle KH. Behavior of concrete under biaxial stresses. ASCE J Eng Mech Div 1973;99:853–66.

[50] Ribas C, Cladera A. Resistencia a cortante de los forjados de vigueta pretensada y bovedilla. Universitat Politècnica de Catalunya, 2013.

Appendices

These appendices contain further information that is not provided in the main body of the paper for sake of brevity.

Appendix A. Nomenclature

a	shear span
A_{sl}	area of the cross-section of the slab's longitudinal reinforcement
A_{sw}	area of the cross-section of the two legs of a stirrup
b	web width of the concrete section
b_{eff}	slab's effective shear width
d	effective depth
d'	slab's longitudinal reinforcement depth
d_b	precast beam's effective depth
d_c	the entire composite beam's effective depth
E_c	concrete's modulus of elasticity
E_s	modulus of elasticity of reinforcement
$f_{c,28}$	compressive strength of the concrete measured in cylinders at the age of 28 days
$f_{c,b}$	compressive strength of the beam's concrete measured in cylinders
$f_{c,s}$	compressive strength of the slab's concrete measured in cylinders
$f_{c,wa}$	weighted average of the beam and slab's concrete compressive strengths measured in cylinders estimated from the area ratio
f_{ct}	concrete's tensile strength

1	$F_{H,i}$	horizontal force transferred at the nodes located on the interface crack
2	$F_{i,nc}$	horizontal force at the interface of the principal span that was not cracked before
3		V_{ic}
4	f_u	tensile strength of reinforcement
5	f_y	yield strength of reinforcement
6	h_s	cast-in-place slab height
7	$l_{i,nc}$	length of the interface of the principal span that was not cracked before V_{ic}
8	N_s	axial force in the slab
9	$\emptyset$	nominal diameter of a reinforcing bar
10	T_l	tension force of slab longitudinal reinforcement
11	T_w	tension force of web reinforcement
12	V	shear force
13	V_{exp}	experimental shear strength
14	V_{ic}	shear force at which the interface crack clearly extended along the interface
15	V_{pb}	the precast beam's shear strength
16	V_{pred}	the specimen's predicted shear strength value
17	V_s	slab shear strength
18	$V_{s,BF}$	slab shear strength provided by the slab bending failure
19	$V_{s,IF}$	slab shear strength provided by the interface failure
20	$V_{s,SF}$	slab shear strength provided by the slab shear failure
21	γ_c	partial safety factor for the concrete material properties

1	γ_s	partial safety factor for the steel material properties
2	ε_c	strain on the concrete surface
3	$\varepsilon_{s,i}$	average strain of stirrup i
4	$\varepsilon_{s,l}$	tension longitudinal reinforcement strain below the point load
5	ε_u	reinforcement strain at the maximum load
6	ε_y	reinforcement strain at yield strength
7	θ	angle between the strut and the axis of the member
8	ρ_l	reinforcement ratio of tension longitudinal reinforcement
9	ρ_w	reinforcement ratio of web reinforcement
10	σ_1, σ_2	principal stresses
11	σ_x	normal stress in the longitudinal direction
12	τ	tangential stress
13	$\tau_{i,exp}$	experimental shear stress at the interface between concretes

14 Appendix B. Summary of the mechanical model proposed by Rueda-
15 García et al. [24]

16 Three variants of the proposed model are distinguished depending on the interface crack
17 extension along the principal span. Fig. B.1 depicts the three variants in examples of the test
18 specimens in this experimental programme.

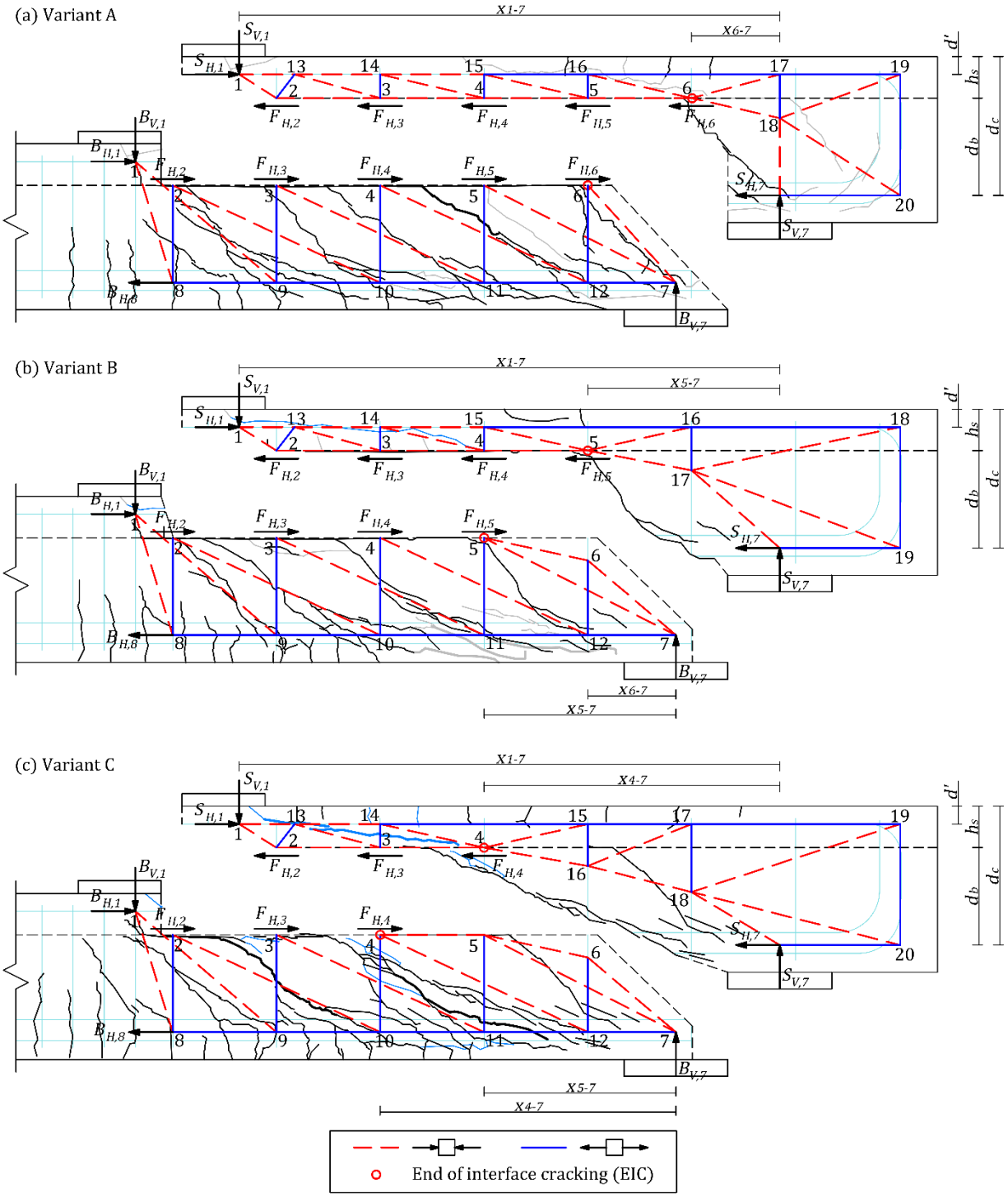

Fig. B.1. Proposed strut-and-tie models for the precast beam and the cast-in-place slab separately: (a) Variant A (specimen HWP5D2); (b) Variant B (specimen HWP5C2); (c) Variant C (specimen HWP6C1).

Shear strength is estimated as the sum of the shear force transmitted along each load path (the precast beam and the cast-in-place slab):

$$V_{pred} = B_{V,7} + S_{V,7} = V_{pb} + V_s = V_{pb} + min\{V_{s,BF}, V_{s,SF}\} \quad \text{(B.1)}$$

The formulation to obtain these variables based on the strut-and-tie models of Fig. B.1 is summarized in Table B.1. The shear transmitted by the precast beam is limited by the yielding of stirrups' steel. Accordingly, the shear transmitted by precast beam V_{pb} is obtained, as are the horizontal forces that balance nodes i in Fig. B.1 ($F_{H,i}$), which represent the dowel action of the transverse reinforcement and the aggregate interlock at the cracked interface. The slab's strut-and-tie model receives these horizontal forces $F_{H,i}$, which have equal values and opposite directions (Fig. B.1). Two possible slab failure mechanisms are calculated. Firstly, slab bending failure due to the slab's longitudinal reinforcement ($V_{s,BF}$) yielding. In this case, horizontal ties 16-17, 15-16 or 14-15, in Variant A, B and C, respectively (Fig. B.1), are considered to yield. Secondly, slab shear failure ($V_{s,SF}$), in which case the slab is considered to be subjected to a biaxial state of stresses, and failure occurs when concrete principal stresses reach Kupfer's failure envelope [49]. The shear force transmitted through the slab (V_s) will be the lowest of the shear forces resisted by each mechanism. For a detailed explanation of the origin of each formula, see [24].

Table B.1. Formulation for obtaining the shear strength transmitted through the precast beam and the cast-in-place slab.

Variable	Variant of the model	Formulas
$F_{H,i}$	A	$T_w = A_{sw} \cdot f_y$ $F_{H,i} = T_w \cdot \cot\theta_i$, where $i = 2, 3, 4, 5, 6$
	B	$T_w = A_{sw} \cdot f_y$ $F_{H,i} = T_w \cdot \cot\theta_i$, where $i = 2, 3, 4$ $F_{H,5} = \frac{T_w(x_{5-7} + x_{6-7})}{d_b}$
	C	$T_w = A_{sw} \cdot f_y$ $F_{H,i} = T_w \cdot \cot\theta_i$, where $i = 2, 3$ $F_{H,4} = \frac{T_w(x_{4-7}+x_{5-7})}{d_b}$
V_{pb}	All	$V_{pb} = B_{V,7} = 2T_w$
$V_{s,BF}$	All	$T_l = A_{sl} \cdot f_y$ $V_{s,BF} = S_{V,7} = \frac{\left(\sum_{i=2}^{K} F_{H,i}\right) \cdot (h_s - d') \cdot d_b + T_l \cdot (h_s - d') \cdot (d_c - d')}{x_{1-7} \cdot d_b - x_{K-7} \cdot (d_c - d')}$
$V_{s,SF}$	All	$N_s = F_{H,K} + \frac{V_{s,SF} \cdot x_{1-7} - (h_s - d') \cdot \sum_{i=2}^{K} F_{H,i}}{d_c - d'}$ $\sigma_x = -\frac{N_s}{b_{eff} \cdot h_s}$ $\sigma_1 = \frac{\sigma_x}{2} + \sqrt{\left(\frac{\sigma_x}{2}\right)^2 + \tau^2} \leq f_{ct}$ (1) $\sigma_2 = \frac{\sigma_x}{2} - \sqrt{\left(\frac{\sigma_x}{2}\right)^2 + \tau^2} \geq -f_{c,s}$ (2) Substitute (1) and (2) in $\sigma_1 = \lvert f_{ct}\rvert + 0.8\frac{\lvert f_{ct}\rvert}{\lvert f_{c,s}\rvert}\sigma_2 \rightarrow Solve\ \tau$ $V_{s,SF} = 2/3 \cdot \tau \cdot b_{eff} \cdot h_s$

Forces $F_{H,i}$ are considered positive in the direction indicated in Fig. B.1.
x_{j-k} is the horizontal distance between nodes j and k in Fig. B.1.
θ_i is the angle between the strut that converges at node i and the axis of the member.
K is the identifier of the node located at the end of interface cracking (EIC in Fig. B.1).
The other variables are defined in Appendix A: Nomenclature.

Appendix C. Calculating the experimental interface shear strength

The experimental shear strength of the interface ($\tau_{i,exp}$) is estimated from the horizontal forces equilibrium in the slab strut-and-tie model of Variant C (Fig. C.1). The shear force resisted by the slab ($S_{V,1}$) is calculated as the difference between the experimental shear force at interface cracking (V_{ic}), which is the V_{exp} in the specimens with interface failure, and the shear strength of the precast beam (V_{pb}). With the $S_{V,1}$ value, the horizontal force at slab $S_{H,1}$ is calculated as:

$$S_{H,1} = \frac{\sum_{i=2}^{4} F_{H,i} \cdot d_b + S_{V,1} \cdot x_{1-7}}{d_c - d'} \quad (C.1)$$

where horizontal forces $F_{H,I}$ are calculated following the procedure described in Appendix B.

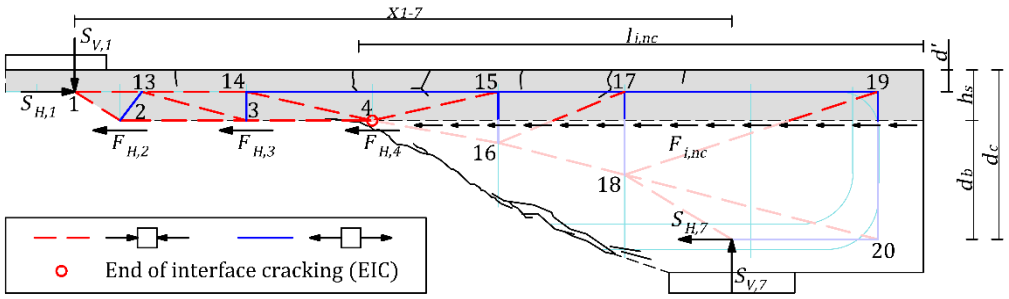

Fig. C.1. Isolated slab in the strut-and-tie model of the cast-in-place slab of Variant C.

The horizontal force at the uncracked interface (Fig. C.1) is calculated as:

$$F_{i,nc} = S_{H,1} - \sum_{i=2}^{4} F_{H,i} \tag{C.2}$$

Interface shear stress $\tau_{i,exp}$ is obtained as a distributed force in the uncracked interface area:

$$\tau_{i,exp} = \frac{F_{i,nc}}{b \cdot l_{i,nc}} \tag{C.3}$$